AIAA

AIAA 2003-0980

In Search of the Physics: The Interplay of Experiment and Computation in Slat Aeroacoustics

Mehdi R. Khorrami, Meelan Choudhari, Bart A. Singer,
David P. Lockard, and Craig L. Streett

NASA Langley Research Center
Hampton, Virginia

41st Aerospace Sciences Meeting & Exhibit
January 6–9, 2002
Reno, Nevada

In Search of the Physics:
The Interplay of Experiment and Computation in Slat Aeroacoustics[*]

Mehdi R. Khorrami[1]
Meelan Choudhari[2]
Bart A. Singer[3]
David P. Lockard[2]
Craig L. Streett[4]

NASA Langley Research Center
Hampton, Virginia

Abstract

The synergistic use of experiments and numerical simulations can uncover the underlying physics of airframe noise sources. We focus on the high-lift noise component associated with a leading-edge slat; flap side-edge noise is discussed in a companion paper by Streett et al. (2003). The present paper provides an overview of how slat noise was split into subcomponents and analyzed with carefully planned complementary experimental and numerical tests. We consider both tonal and broadband aspects of slat noise. The predicted far-field noise spectra are shown to be in good qualitative (and, to lesser extent, good quantitative agreement) with acoustic array measurements. Although some questions remain unanswered, the success of current airframe noise studies provides ample promise that remaining technical issues can be successfully addressed in the near future.

Introduction

The negative effects of aircraft noise in communities adjacent to airports can severely curtail future growth in civil air travel. Adverse impacts of noise extend well beyond local concerns. Noise restrictions may also impact the nations' economy via imposed flight curfews and other limitations. To help reduce this impact, one of NASA's stated goals in the field of aeronautics is to reduce perceived aircraft noise emissions by a factor of two (10 dB) within ten years and a factor of four (20 dB) within twenty-five years. To achieve these ambitious goals, significant advances in noise prediction and suppression technologies must be realized.

Airframe noise is most pronounced during aircraft approach and landing because engines are operating at reduced thrust and high-lift devices and landing gears are deployed. Moreover, during approach, aircraft fly at a relatively shallow glide slope; flying at low elevations for long periods of time exposes ground communities to extended durations of higher noise. NASA, in collaboration with industrial and academic partners, has embarked on a major research program to enhance our fundamental understanding of airframe noise sources and to apply this knowledge to develop noise reduction technologies that are both effective and aerodynamically efficient. This effort involves a synergistic combination of computations and experiments. In this paper, we present an overview of the major noise mechanisms associated with a leading-edge slat, with an emphasis on the important role of computational simulations in identification and understanding of noise sources underlying the experimentally measured airframe noise spectra. These simulations span a wide range of flow phenomena and modeling approximations, including 2-D, 3-D, steady, and unsteady flow fields.

The geometric and aerodynamic complexity of high-lift components has precluded a fundamental understanding (and, hence, control) of the associated noise sources. The existing prediction techniques rely on semi-empirical curve fits (e.g., the Fink (1979) model) based on a limited knowledge of the actual noise source mechanisms. More importantly, existing techniques fail to describe some of the causal dependencies that are vital for effective abatement of airframe noise radiation. The NASA airframe noise team, which was first assembled under the Advanced Subsonic Technology (AST) program, and has continued its efforts under the Quiet Aircraft Technology (QAT) program, has the goal to develop a second-generation prediction methodology that incorporates a tighter coupling between the radiated far-field noise and the fundamental fluid mechanics of unsteady near-field disturbances in the flow past various airframe components. To achieve this goal, the NASA program launched a systematic investigation involving a complementary set of experiments and computations that spans the entire cause-effect chain related to airframe noise. Macaraeg (1998) provides an overview of the airframe noise work conducted at NASA Langley Research Center (LaRC) prior to 1998. The synergistic use of experiment and computation as it relates to flap side-edge noise research is discussed in a companion paper by Streett et al. (2003). In the present paper, we devote our attention to some of NASA's recent accomplishments related to leading-edge slat noise. We emphasize, however, that our omission of other experimental and computational efforts should by no means diminish the significant contributions that have been made by other institutions both in the US and Europe.

Slat High-Frequency Noise

Under the AST program, the first set of experimental measurements involving a generic high-lift system were obtained at NASA Ames Research Center. The unswept three-element high-lift configuration was composed of a main element, a leading-edge slat, and a part-span flap. In a stowed position, the model had a chord of 0.76 m with slat and flap chords accounting for 15 and 30%, respectively. In a series of tests in the 7x10 ft tunnel, acoustic array measurements provided the noise source localization maps as well as the acoustic spectra for the slat. Storms et al. (1998) provide a detailed account of the studies. Slat acoustic spectra from the Ames measurements are shown in Fig.1; results for low and high slat deflection angles are plotted. The spectrum for the 26-deg slat deflection (a typical landing

configuration) shows high levels of noise between 10 and 22 kHz with a center frequency of 15 kHz. Interestingly, the noise spectrum in Fig. 1 possesses elements of both tonal and broadband noise. At low slat deflections, the high-frequency tonal hump virtually disappears. Although not shown in the figure, at the higher slat deflection, the tonal hump is removed when the gap is zeroed and taped over. Based on this observation, Storms et al. (1998) attribute the tonal hump in the spectrum to the slat gap (gap noise) but they provide no definitive physical mechanisms for noise generation.

Shortly after the Ames tests, additional airframe noise experiments were performed in the LaRC Low Turbulence Pressure Tunnel (LTPT); see Choudhari et al. (2002a). As a pressurized tunnel, the LTPT provided an opportunity to test at a variety of Reynolds numbers in a range approaching flight values. The test model was an energy efficient transport (EET) wing with a realistic sectional profile. The unswept three-element EET wing was composed of a slat, a supercritical main element, and a flap. The model had a stowed chord of 0.55 m and the slat and flap chords were 15.5% and 30%, respectively. During separate tunnel entries in 1998 and 1999, acoustic and limited on-surface aerodynamic measurements were obtained. The initial 1998 entry included a part-span flap. In the 1999 entry, the part-span flap was replaced with a full-span flap with a slightly different profile. The full-span flap eliminated a dominant source of noise associated with the flap side edge and thereby improved the signal-to-noise ratio associated with the slat acoustic sources. Important parameters such as the slat geometry, settings, and aerodynamic loading were unchanged for the entry during 1999, and the corresponding radiated sound fields remained nearly identical. The EET model with the part-span flap and its cross-sectional profile are shown in Fig.2.

Sample microphone array measurements of the EET slat at two distinct slat deflections from 1998 entry are displayed in Figs. 3 and 4. The measured acoustic data, processed in 1/12-octave bands, span a wide range of Reynolds numbers. For the 30-deg slat deflection, the measurements show high-amplitude sound in the lower range of frequencies, followed by a gradual drop in the sound levels in the mid-frequency band. In the vicinity of 40–50 kHz, the spectra display a broad tonal behavior. The sound pressure levels of this tonal hump were so severe that for certain combinations of slat settings and test conditions, they virtually masked any other sources of noise. Except for a weak dependency of the tonal noise, the slat noise remained mostly

independent of the Reynolds number. At the lowest Reynolds number, the tonal peak occurred at a slightly lower frequency (approximately 42 kHz) and had an amplitude that was 30–50% lower than the measured amplitude at the highest Reynolds number. At a slat deflection of 20 deg (Fig. 4), the sound levels are considerably lower than the corresponding 30-deg case. In a trend that mimics the Ames studies in the 7x10 ft tunnel, the tonal hump at high frequency nearly disappears with the lowering of the slat angle. With hindsight, it is easy to see similar patterns and behavior of the noise spectra from the two tests. Initially, however, such a connection was not so obvious: the LaRC model size was 30% smaller than the Ames model, yet this reduction shifted the center frequency of the broadband tonal noise by nearly 400%.

In an effort to better understand the origin of the high-frequency noise and to test the prevailing hypotheses at that time (gap noise, gap resonance, acoustic feedback, etc.), the airframe noise team performed additional tests with the EET model. In those tests, the gap and the overhang for the slat were varied over a limited range, and no appreciable shift in the high-frequency source occurred. Furthermore, examination of the measured acoustic data at other Mach numbers (Fig. 5) verified the occurrence of the high-frequency hump at a fixed Strouhal frequency. These observations suggested that the high-amplitude tonal component is, to first order, caused by some hydrodynamic phenomena (such as shedding) and not by an acoustic resonance mechanism. The measured spectra at several Mach numbers for a slat deflection of 30 deg and Reynolds number of 7.2 million are plotted in Fig. 5. The frequency axis is normalized to M=0.2 using Strouhal scaling. Using V^5 scaling, a reasonable collapse of the data in the high-frequency range is achieved. The collapse at the low frequencies, however, is poor.

During the 1998 LTPT entry, in addition to the acoustic data, some on-surface pressure measurements (static pressure ports, pressure sensitive paint) of the EET model were obtained. However, due to the pressurized environment and tunnel entry time limitations, detailed off-surface aerodynamic measurements were neither feasible nor cost effective. Therefore, a deeper connection between the near-field fluid dynamic phenomena and the slat far-field acoustic signature remained partially unanswered. To remedy this shortcoming, a series of computations that were carefully tailored to simulate the EET flow field in the LTPT environment, were planned and executed (see Berkman et al. 2000).

The initial set of Reynolds-averaged Navier-Stokes (RANS) computations involved the full three-element, part-span flap model. These simulations, conducted in the steady, fully turbulent mode, were geared towards resolving and isolating the mean flow features that could either produce or support local unsteady fluctuations. To simplify the computational task and to speed up convergence, all blunt trailing edges were replaced with sharp edges. A sample plot in Fig.6, taken from Berkman et al. (2000), shows a comparison between the measured and computed chordwise pressure distribution over the three-element EET model. Excellent agreement was obtained. A dominant but known flow feature highlighted by the steady flow field was the free shear layer that forms at the cusp (caused by boundary layer separation) and reattaches to the slat undersurface near the trailing edge. As an efficient amplifier of the background disturbance field, the shear layer was considered likely to be the fluid dynamic mechanism responsible for the broadband tonal noise in the spectra. However, a linear stability analysis of the shear layer velocity profiles in the vicinity of the cusp failed to support this speculation. The stability analysis produced amplifying disturbances that were in a frequency band less than 12 kHz. Clearly, the shear layer could not support the tonal noise that had a center frequency of 48 kHz.

During informal discussions in 1998 (after the initial LTPT tests), the airframe noise team further considered the conjecture that Strouhal shedding at the slat trailing edge was the underlying mechanism for the high-amplitude tonal sound. This speculation was initially based on the slat's design with a trailing-edge thickness of 0.39 mm. Using freestream velocity and the edge height, an assumed Strouhal number of St = 0.22 provided a shedding frequency of nearly 40 kHz, a calculation that seemed to agree with the measured center frequency. After the initial skepticism about the bluntness of the trailing edge, as one co-worker was cut by the sharp trailing edge while handling the slat in the tunnel, careful measurements revealed that the manufactured slat had a thickness of 0.5 mm. Moreover, new measurements by colleagues at NASA Ames revealed that the trailing-edge thickness of the 7x10 ft model was 2.2 mm, which is four times the thickness of the EET model. The ratio of the trailing edges of the two tests thus was consistent with the 400% shift in center frequency of the tonal hump (see Figs. 1 and 5).

To investigate the vortex shedding conjecture, Khorrami et al. (2000) performed unsteady Reynolds-averaged Navier-Stokes (URANS) computations of the EET high-lift system. Because the tested slat covered the

entire tunnel span, the simulations were limited to a 2-D configuration. For these simulations, the treatment of the trailing edge bluntness was a crucial and challenging step. To accurately predict the slat's vortex shedding, the computational trailing-edge geometry matched the actual thickness rather than being idealized as a sharp edge. For the high-lift computations, the capturing of the slat wake and its downstream evolution is of primary importance. To accomplish this task, extremely fine grids and significant mesh clustering were employed at the trailing edge.

The computed instantaneous spanwise vorticity field at the slat trailing edge (Khorrami et al. 2000) is shown in Fig. 7. The established vortex street is clearly displayed and confirms the conjectured vortex shedding at the trailing edge. Because of the coarsening spatial resolution beyond two vortex diameters downstream of the trailing edge, the convected vortices decay rapidly farther downstream. Analysis of the unsteady pressure field revealed a purely periodic signal in the vicinity of the edge. The highest amplitude pressure fluctuations occur at the edge, specifically at the two sharp corners. Fourier analysis of the pressure signal at the two corners and other nearby locations indicated a shedding frequency of approximately 39 kHz, which is within the range of the measured frequencies of the hump shown in Fig. 3. The propagating waves and the established wave patterns near the slat's trailing edge and cove areas are shown in Fig. 8. Of particular significance is the reflection of the wave at the leading edge of the main element, which results in a distinct interference pattern across the gap and in the cove area.

In a separate study, Singer et al. (2000) used an acoustic analogy (the Ffowcs Williams and Hawkings equation) to compute the far-field acoustics from the time records of the URANS computations. Both on-surface and off-surface integration was employed. The computed directivity patterns showed significant lobes directly upstream of the slat and downward toward the microphone array (ground). In fact, the downward directivity pattern was used to better position the array location for the second entry in 1999. Overall, the agreement between the computed far-field acoustics and the array measurements supports the conclusion that the simulated near-field flow dynamics was sufficiently accurate.

Additional simulations (Khorrami et al. 2000) were carried out to check if the shedding phenomenon would also explain some of the measured trends (Figs. 3 and 4) in the acoustic spectrum for the high-amplitude peak. To that end, URANS computations at a slat deflection of 20 deg were performed. At the lower slat deflection, no vortex shedding at the trailing edge was observed; thus the trend displayed in Fig. 4 was corroborated. Moreover, in additional calculations, the reduction in amplitude and the shift to a lower shedding frequency with decreasing Reynolds number were also reproduced numerically. Follow-on experimental studies, conducted at both NASA and elsewhere, have since firmly established the presence of vortex shedding at the slat trailing edge. Notable among those studies are Storms et al. (1999), Olson et al. (2000, 2001), Takeda et al. (2002), and Mendoza et al. (2002).

Slat Low- and Mid-Frequency Noise

After the companion computational simulations revealed the responsible mechanisms for some of the slat noise sources (in particular the trailing-edge vortex shedding), a more focused acoustic study of the EET slat was initiated during the 1999 entry. For that entry, large and small aperture arrays were employed to measure the low- and high-frequency noise, respectively.

The slat acoustic spectra at several angles of attack are displayed in Fig. 9. The 6- and 9-deg results are from the 1999 entry. Due to the lack of measurements for the same settings and conditions at higher angles of attack, the 15-deg spectrum is taken from the 1998 entry. Acoustic amplitudes in the lower frequency bands increase substantially with decreasing angle of attack. On the other hand, the high-frequency tonal noise reveals no distinct patterns.

Once the source mechanism for the high-frequency noise was determined, the focus shifted to understanding the sound sources in the lower frequency band of the slat acoustic spectra. Although geared towards resolving the trailing-edge flow field, the earlier URANS solution pointed to the presence of additional flow oscillations in the slat-cove region. The observed oscillations were associated with the slat free shear layer and had frequencies between 2 and 4 kHz. This observation and previous linear stability analysis pointed to the noise generation role of large-scale instability modes of the slat shear layer. A similar conclusion was drawn by Dobrzynski et al. (1998), based on an extensive aeroacoustic testing of a European designed high-lift system. Two concurrent aerodynamic studies (unrelated to our airframe noise effort) further supported this conjecture. Using particle image velocimetry (PIV), Paschal et al. (2000) mapped the flow field slightly downstream of the slat trailing edge of a similarly configured high-lift system. At a low

angle of attack (4 deg), the PIV-generated images showed the presence of large, strong spanwise vortices in the slat's wake. Size and location of these rollers relative to the wake preclude the slat trailing edge as the source. Most likely, as pointed out by Paschal et al., these vortices originate from the slat-cove region and then are pumped through the gap. As the angle of attack increases, unsteadiness leaving the cove is diminished, and the number of vortices in the wake is significantly reduced. Similarly, Takeda et al. (2001) employed the PIV technique to map the flow field inside a slat-cove area of a European designed high-lift system. The growth of shear layer disturbances and their subsequent evolution into large-scale coherent structures were captured.

The next series of URANS simulations, conducted by Khorrami et al. (2002a), tested the conjecture that amplified perturbations in the free shear layer are responsible for the low-frequency content of the slat acoustic spectra. To properly resolve the shear layer and accurately capture the evolution of the large-scale structures, the number of grid points in the slat-cove region and the surrounding area was significantly increased. Similar to the trailing-edge noise studies, the computational framework of URANS plus the Ffowcs Williams and Hawkings formulation was followed to calculate the far-field acoustics.

The fully turbulent simulations of Khorrami et al. (2002a) required explicit forcing of the shear layer to excite and maintain the large-scale structures. Figure 10 shows an instantaneous shot of the spanwise vorticity field in the slat-cove area for the fully turbulent forced case. The vorticity contours display the spatial location of the free shear layer. The shear layer is a good amplifier of the initial perturbations that grow rapidly, roll up the shear layer, and form discrete vortices. However, the fully turbulent computations proved to be overly diffusive; the rolled-up vortices rapidly decayed within a short spatial distance (Fig. 10). This premature diffusion prevented proper development of the cove flow field, disallowed the vortices to escape through the gap, and artificially decreased the radiated acoustic signature. Although better agreement with experimental measurements remained desirable, the computations reinforced the speculation that amplification of shear layer instabilities produces the radiated noise in the lower frequency range.

To circumvent the excessive diffusive effects of the turbulence model, a simple zonal approach based on physical arguments was advocated and pursued by Khorrami et al. (2002b). They argued that in the cove region, the established flow field is quasi-laminar but highly unsteady. Accordingly, the production term associated with the turbulence model was switched off in a limited zone that enclosed the cove area. A sample plot of the instantaneous spanwise vorticity field from the partially laminar simulation at an 8-deg angle of attack is shown in Fig. 11. In contrast to the fully turbulent simulations, the cove region displays extremely complex and highly nonlinear flow dynamics. Important stages, such as shear layer oscillation, roll-up, and the formation of discrete vortices, are vividly depicted. Another important distinction is that unlike the fully turbulent case, the shear layer is self-exciting and no external forcing was used. A snapshot of the vorticity field for the 6-deg case is displayed in Fig. 12. The figure clearly shows the ejection process through the gap of several vortices (carrying negative vorticity) and some positive vorticity lumps. The ejected vorticity field is spread over a significant portion of the gap width. These observations corroborate the PIV measurements obtained at angles of attack of 4 and 5 deg by Paschal et al. (2000) and Takeda et al. (2001). Another prominent feature in Fig. 12 is the presence of a very large and strong vortex of positive vorticity near the center of the recirculating zone. The center vortex produces low-frequency (less than 1000 Hz) oscillations. The existence of such prominent vortex has not been observed in the limited PIV data available. Although the low frequency oscillations may be acoustically irrelevant in a full scale environment, nevertheless, the presence of the center vortex greatly alters the dynamic of the cove flow field and thus requires further exploration.

Unsteady flow data were used as input for the solution of Ffowcs Williams and Hawkings equation to calculate the noise radiated below the high-lift system. A sample of the computed and measured acoustic spectra for the 6-deg case (Khorrami et al. 2002b) is displayed in Fig. 13 (measured spectrum is from 1999 LTPT entry). The shape of the spectrum over the entire frequency band (including the shedding frequency) is well captured. The decay with frequency and the frequency of the noise minimum are similar for the computation and experiment. The higher acoustic amplitude in the predicted spectrum is due to the perfect spanwise correlation assumed for the near-field unsteady signal. In an actual experiment, three-dimensional effects provide a spanwise correlation that is less than perfect. Therefore, a two-dimensional acoustic computation potentially overestimates the noise significantly. The magnitude of this overestimation is an open question that needs to be resolved. Computed acoustic spectra for three angles of attack are shown in Fig.14. In

accordance with measured trends (Fig. 9), decreasing the angle-of-attack produces higher acoustic amplitudes.

In an effort to better understand the causalities between the near-field fluctuations in the cove and the radiated sound field, Choudhari et al. (2002b) carried out additional simulations. Based on the research community's experience with jet noise, regions of high-amplitude turbulent kinetic energy (TKE) are likely hot spots where mechanical energy is converted into acoustic energy. Extensive analysis of the URANS solutions revealed higher TKE magnitude within the cove region. The computed TKE data have the same features as the experimental measurements (Takeda et al. 2001): namely, higher TKE levels in the shear layer, in the recirculating flow along the slat pressure surface , and in the vicinity of the shear layer reattachment location. Intense near-field fluctuations in the simulated flow were identified with unsteady separation along the slat bottom surface, relatively close to the slat cusp. This particular feature could not be corroborated by the limited measurements available. Thus, the accuracy of the laminar cove simulations in this near-wall region remains an open issue.

Additional simulations for $M = 0.1$ and $M = 0.3$ were used to determine the velocity scaling laws for the computed noise. According to Choudhari et al. (2002b), the computed acoustic spectra for an observer at 90 deg below the wing appear to follow the V^4 acoustic power law (Fig. 15). Once again, the frequency axis is normalized to $M = 0.2$ using Strouhal scaling. Recall that the measured acoustic spectra at similar angles of attack were scaled according to the V^5 law (Fig. 5). The lower exponent used for the computed noise levels is consistent with the 2-D nature of the flow simulation and the acoustic calculation. The 3-D nature of acoustic sources in the real flow would result in a V^5 scaling. The nature of the collapse in Fig. 15 is similar to that of the measured data (Fig. 5), which suggests that the simulations are roughly consistent with yet another crucial parametric trend.

Summary

Increasingly, numerical simulations are becoming an integral part of aeroacoustic research. This increased prevalence is due to the convergence of several related factors: notably, the maturing of an array of flow solvers, the availability of powerful yet cheap commodity computer hardware, limited tunnel entry time in facilities where detailed aeroacoustic measurements can be made, and the availability of wind

tunnel environments that are suitable for only aerodynamic investigations. Based on these emerging factors, state-of-the-art measurement and simulation techniques must be used interchangeably to fill the existing gaps in aeroacoustic knowledge. Use of these advanced tools is necessary to construct a deeper understanding of airframe noise sources and to develop noise source models and noise suppression technologies.

In this paper, we have presented a brief account of the intertwined and complementary set of experiments and computations aimed at the noise source mechanisms associated with a slat. The slat noise component in itself is a complex aeroacoustic problem that involves a combination of interdependent noise generation mechanisms in overlapping frequency bands. A variety of experiments and simulations that were performed to address both tonal and broadband aspects of slat noise have been discussed. It was shown that good qualitative and in some cases good quantitative agreement between the measured and computed acoustic spectra can be obtained. Although absolute acoustic levels cannot be predicted with any level of certainty, the apparent success of present airframe noise studies holds the promise that some of the remaining technical issues will be addressed successfully in the near future.

References

Berkman, M.E., Khorrami, M.R., Choudhari, M., and Sadowski, S.S., " Investigation of High-Lift Flowfield of and Energy Efficient Transport Wing, " J. of Aircraft, Vol.37, No.1, pp. 45-52, Jan.-Feb. 2000.

Choudhari, M., Khorrami, M.R., Lockard, D.P., Atkins, H., and Lilley, G., " Slat Cove Noise Modeling :A Posteriori Analysis of Unsteady RANS Simulations, " AIAA Paper 2002-2468, June 2002b

Choudhari , M., et al., "Aeroacoustic Experiments in the Langley Low –Turbulence Pressure Tunnel, " NASA TM-2002-211432, Feb. 2002a.

Dobrzynski, W., Nagakura, K., Gehlhar, B., and Buschbaum, A., "Airframe Noise Studies on Wings with Deployed High-Lift Devices," AIAA Paper 98-2337, 1998.

Fink, M.R., "Noise Component Method for Airframe Noise," J. Aircraft, Vol.16, No. 10, pp. 659-665, 1979.

Khorrami, M. R., Berkman, M. E., and Choudhari, M., "Unsteady Flow Computations of a Slat with a Blunt Trailing Edge," AIAA J., Vol. 38, No. 11, November, pp. 2050-2058, 2000.

Khorrami, M. R., Singer, B. A., and Berkman, M. E., "Time-Accurate Simulations and Acoustic Analysis of Slat Free-Shear Layer," AIAA J., Vol. 40, No. 7, pp. 1284-1291, July 2002a.

Khorrami, M. R., Singer, B. A., and Lockard, D.P.., "Time-Accurate Simulations and Acoustic Analysis of Slat Free-Shear-Layer: Part II," AIAA Paper 2002-2579, June 2002b.

Macaraeg, M.G., "Fundamental Investigations of Airframe Noise," AIAA Paper 98-2224, June 1998.

Mendoza, J.F., Brooks, T.F., and Humphreys, Jr., W.M., "Aeroacoustic Measurements of a Wing/Slat Model," AIAA paper 2002-2604, June 2002.

Olson, S., Thomas, F.O., and Nelson, R.C., "A Preliminary Investigation into Slat Noise Production Mechanisms in a High-Lift Configuration," AIAA Paper 2000-4508, 2000.

Olson, S., Thomas, F.O., and Nelson, R.C., "Mechanisms of Slat Noise Production in a 2D Multi-Element Airfoil Configuration," AIAA Paper 2001-2156, May 2001.

Paschal, K., Jenkins, L., and Yao, C., "Unsteady Slat Wake Characteristics of a 2-D High-Lift Configuration," AIAA Paper 2000-0139, January 2000.

Singer, B. A., Lockard, and D. P., Brentner, K. S., "Computational Aeroacoustic Analysis of Slat Trailing-Edge Flow," AIAA J. Vol. 38, No. 9, September, pp. 1558-1564, 2000.

Storms, B.L., Hayes, J.A., Moriarty, P.J., and Ross, J.C., "Aeroacoustic Measurements of Slat Noise on a Three-Dimensional High-Lift System," AIAA Paper 99-1957, May 1999.

Storms, B.L., Ross, J.C., Horne, W.C., Hayes, J.A., Dougherty, R.P., Underbrink, J.R., Scharpf, D.F., and Moriarty, P.J., "An Aeroacoustic Study of an Unswept Wing with a Three-Dimensional High Lift System," NASA TM 112222, Feb. 1998.

Streett, C.L., Lockard, D.P., Singer, B.A., Khorrami, M.R., and Choudhari, M.M., "In Search of the Physics: The Interplay of Experiment and Computation in Airframe Noise Research; Flap-Edge Noise," AIAA Paper 2003-0979, Jan. 2003.

Takeda, K. Ashcroft, G.B, and Zhang, X., "Unsteady Aerodynamics of Slat Cove Flow in a High-Lift Device Configuration," AIAA Paper 2001-0706, January 2001.

Takeda, K., Zhang, X., and Nelson, P.A., "Unsteady Aerodynamics and Aeroacoustics of a High-Lift Device Configuration," AIAA Paper 2002-0570, January 2002.
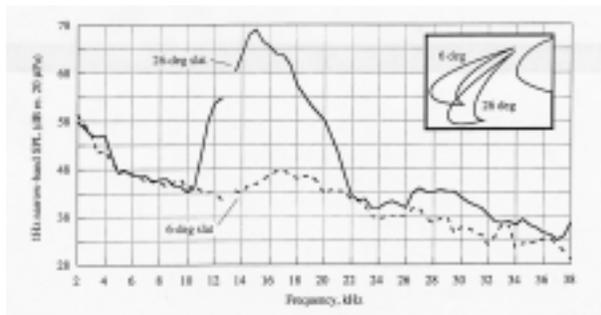
Fig.1 Acoustic spectra at slat deflections of 6 deg and 26 deg for M=0.22 and Reynolds number of 3.7 million based on stowed chord of 0.76m. The horizontal axis indicates model scale frequencies.
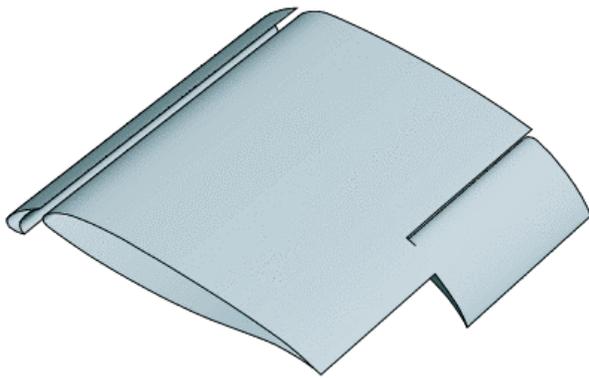
a)   Part-span flap model
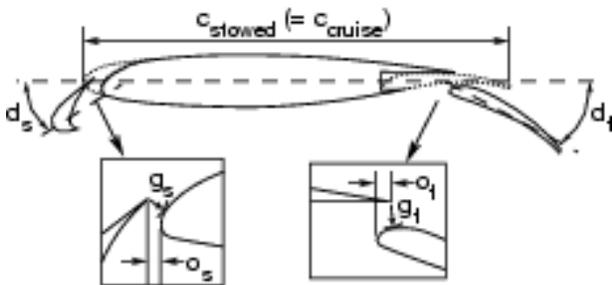
b)   Cross-sectional view

Fig.2   Three-element EET high-lift system. Model stowed chord is 0.55m.
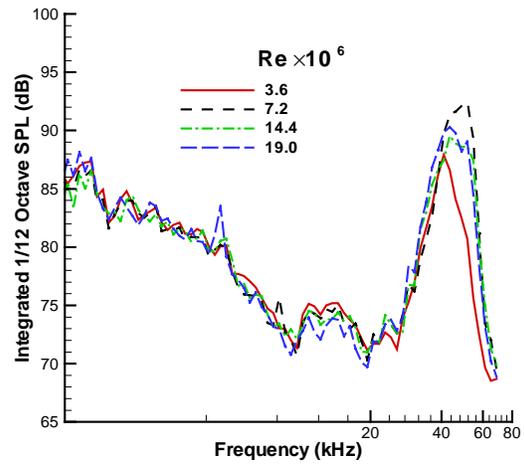
Fig.3   Measured acoustic spectra for EET slat at 30 deg deflection with M=0.2. Reynolds number is based on stowed chord and frequencies are model scale frequencies.
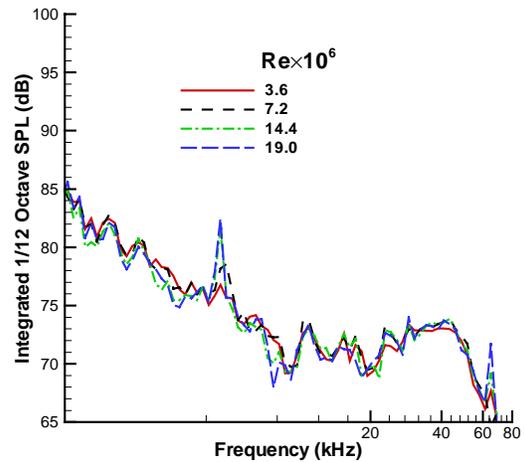
Fig.4   Measured acoustic spectra for EET slat at 20 deg deflection with M=0.2. Reynolds number is based on stowed chord and frequencies are model scale frequencies.
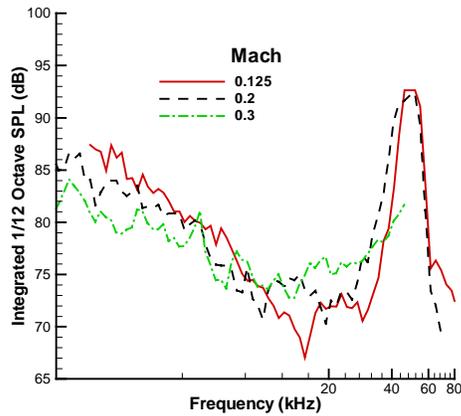
Fig. 5 V^5 velocity scaling of measured noise for 30 deg deflected slat at Re_c=7.2 million. Frequencies are normalized to M=0.2 using Strouhal scaling. SPL's are normalized to M=0.2 using V^5 scaling.
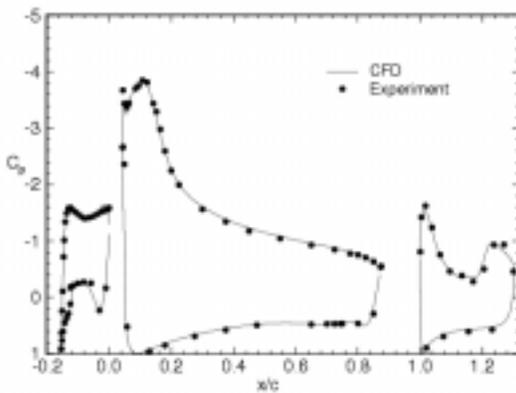
Fig. 6 Chordwise pressure distribution over three-element EET model for slat deflection of 30 deg, angle of attack of 10 deg, flap deflection of 30 deg, M=0.2, and Re_c=7.2 million.
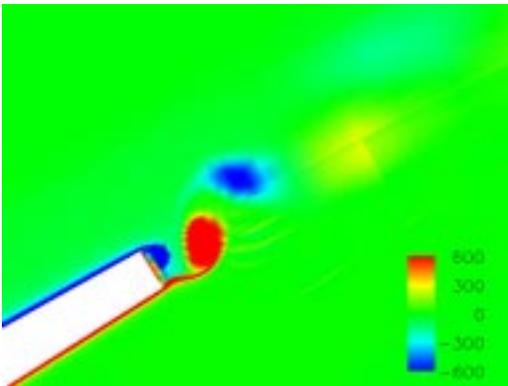
Fig. 7 Instantaneous spanwise vorticity field at slat's trailing edge displaying vortex shedding; slat deflection is 30 deg, M=0.2, and Re_c=7.2 million.
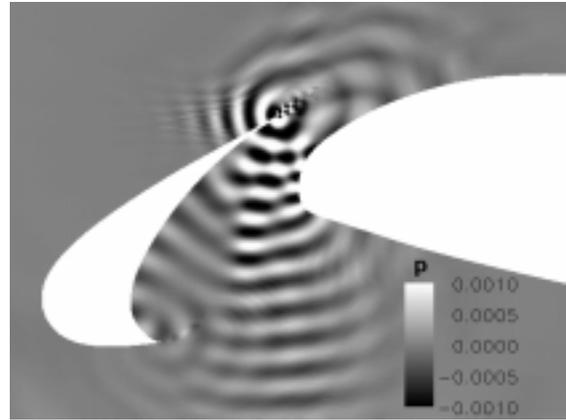
Fig. 8 Instantaneous fluctuating pressure field corresponding to Fig.7. Normalisation is with respect to free-stream density and speed of sound.
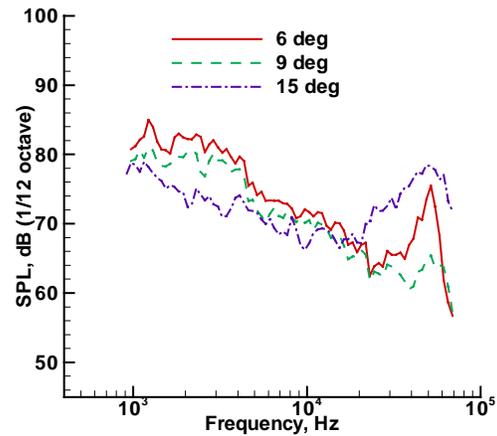
Fig. 9 Variation of measured slat noise with angle of attack at M=0.2 and Re_c=7.2 million. Slat deflection is 30 deg.
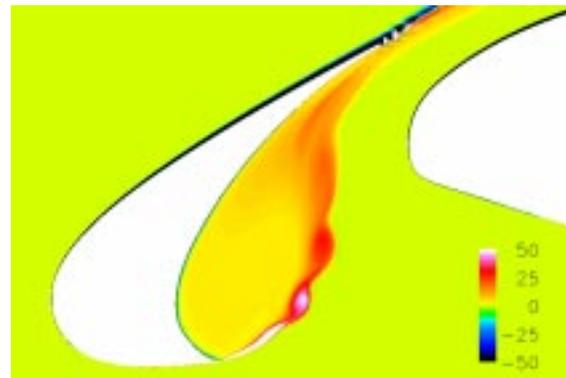
Fig. 10 Simulated instantaneous spanwise vorticity field for fully turbulent forced case; slat deflection is 30 deg, angle of attack 8 deg, M=0.2, and Re_c=7.2 million.

AMERICAN INSTITUTE OF AERONAUTICS AND ASTRONAUTICS

Fig. 11 Simulated instantaneous spanwise vorticity field for partially laminar-cove case. Flow conditions are same as for Fig.10.
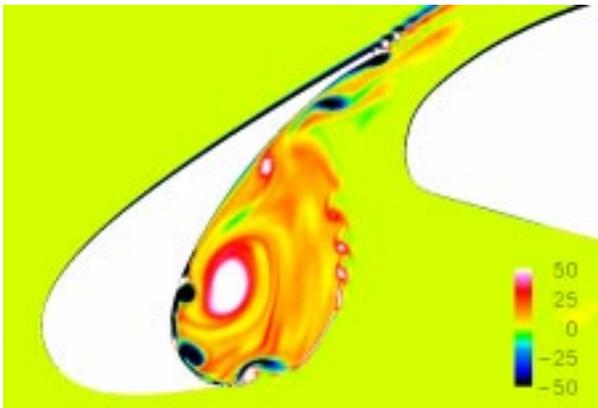
Fig. 12 Simulated instantaneous spanwise vorticity field for partially laminar-cove case. Angle of attack is 6 deg, other conditions are same as in Fig.10.
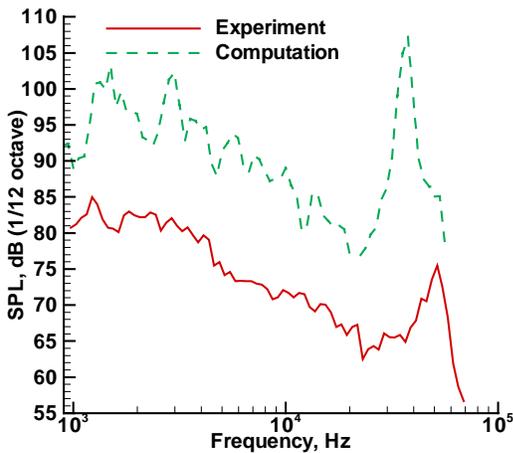
Fig. 13 Comparison of measured and computed acoustic spectra for 30 deg slat in $1/12^{th}$ –octave bands. Angle of attack is 6 deg.
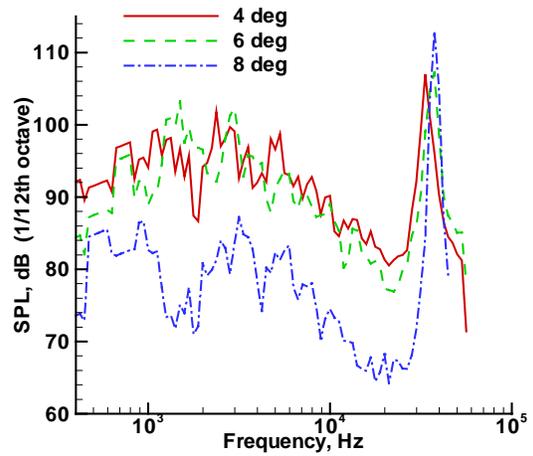
Fig. 14 Variation of computed slat noise with angle of attack at M=0.2 and Re_c=7.2 million. Slat deflection is 30 deg.
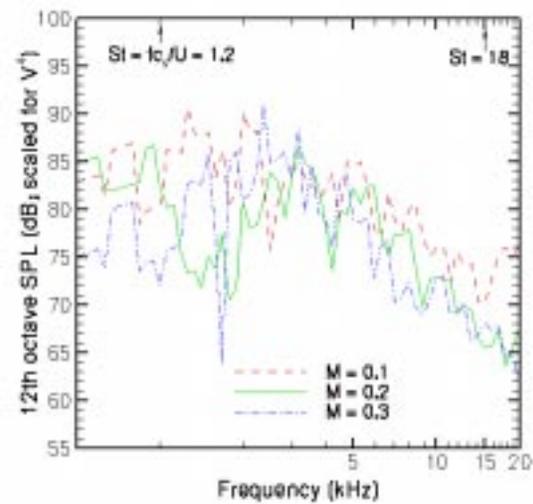
Fig. 15 V^4 scaling of computed noise levels for 30 deg slat at 8 deg angle of attack, M=0.2, Re_c=7.2 million. Strouhal frequency is scaled with respect to slat chord C_s and freestream velocity.

10